Received: 14 March 2022 | Revised: 20 December 2022 | Accepted: 27 January 2023

DOI: 10.1002/rnc.6625

RESEARCH ARTICLE

WILEY

Road preview MPC of semi-active suspension with magneto-rheological damper

Shuyou Yu[1,2] | **Jie Guo**[2] | **Mingsheng Xu**[2] | **Songlin Zhang**[2] | **Ye Zhuang**[1] | **Baojun Lin**[2]

[1]State Key Laboratory of Automobile Simulation and Control, Jilin University, Changchun, Jilin, China

[2]Department of Control Science and Engineering, Jilin University, Changchun, Jilin, China

Correspondence
Shuyou Yu, Department of Control Science and Engineering, Jilin University, Changchun, Jilin, China.
Email: shuyou@jlu.edu.cn

Funding information
National Natural Science Foundation of China, Grant/Award Number: U1964202

Abstract

In this article, a road preview model predictive control scheme for semi-active suspension system with magneto-rheological damper (MRD) is suggested. In order to improve the comprehensive performance of the semi-active suspension, studies of both the actuator and control algorithm have been carried out. For the actuator, e.t. MRD, a cascade control strategy is proposed based on a Hammerstein model, compared with the traditional open-loop control methods, the tracking accuracy of the damping force has been improved. For the control algorithm, in contrast to existing works which define all requirements in a single cost functional and minimize it, in this work a road preview model predictive controller is adopted for semi-active suspension to provide optimal ride comfort by keeping constrained variables within specified limits. The road excitation is a measurable external input rather than an unknown disturbance. Finally, the optimization issue with hard constrains is converted into a quadratic programming problem. Simulation results show that the desired damping force of the MRD is realized by using the cascade control strategy. Meanwhile, vehicles with the proposed road preview model predictive control scheme can achieve better performance compared with a H_∞/generalized H_2 controller.

KEYWORDS

Hammerstein model, magneto-rheological damper, model predictive control, road preview, semi-active suspension, sliding mode control

1 | INTRODUCTION

Suspension connects the vehicle body and the axle elastically, undertakes the force acting between the wheel and the vehicle body. It is usually composed of elastic and damping elements and can be divided into three forms in terms of operation: active, semi-active, and passive.[1] The performance requirements for suspension include: on the one hand, the sprung mass acceleration is required to be as small as possible to improve passenger comfort; on the other hand, the time-domain hard constraints such as suspension stroke, ground-holding requirements and actuator saturation for the handling stability and mechanical constraints should be satisfied.[2] For the passive suspension, the structural parameters are fixed, and its damping and stiffness cannot be adjusted. Therefore, it's difficult to guarantee performance in a changeable environment. Typically, the best performance can be achieved by active suspension. However, active suspension usually needs large power supply, which limits its extensive application in practice. Compared with active suspension system, semi-active

suspension system can provide similar safety and comfort performance while have relatively simple system structure and less power consumption.[3] The semi-active suspension has received increasing attention in recent years, especially, with the development of controllable dampers, such as electro-rheological damper (ERD) and magneto-rheological damper (MRD).[4] Compared with ERD, MRD has advantages of insensitive to impure media, safer, and easier to apply. The disadvantage is that the response time of MRD is slightly longer than that of ERD, but it can be ignored in most engineering applications.[5]

Although MRD has attractive characteristics, the inherent high nonlinearity with hysteresis makes modeling and controller design for MRD a challenging task. The dynamic models of MRD can be divided into direct models and inverse models. The direct models are designed to represent the nonlinear hysteresis characteristics of MRD. The inverse models, as damper controllers, are used to calculate the control current according to the expected damping force, which is significant for the control of semi-active suspension. The current problem with MRD modeling is that the accuracy of parametric models cannot be guaranteed, such as Bing-Ham model,[6,7] revised Bouc–Wen model,[8,9] sigmoid model,[10] nonlinear double viscous model[11] and so forth. Additionally, for nonparametric models, including neural network model,[12,13] polynomial model,[14,15] fuzzy model,[16-18] Hammerstein-Wiener model[19] and so forth the training methods are complex and the solution of currents will take a long time although the modeling accuracy can be improved. Therefore, a model which is accurate and relatively simple of MRD needs to be built. In this article, a Hammerstein model which is composed of a static nonlinear module and a dynamic linear module is proposed for MRD. It has the advantages of low modeling complexity, and can describe the characteristics of the system more accurately. Compared with the Hammerstein-Wiener model,[19] its structure is simpler for controller design.

Open-loop control based on the magneto-rheological inverse model is mainly used in MRD.[20,21] However, the damping force of MRD is strongly dependent on temperature changes, that is, the heat generation caused by friction in the operation of MRD leads to modeling parameter mismatch. For the purpose of improving the control accuracy of MRD, a cascade control strategy is proposed in this article. A static inverse model as a compensator is to offset the nonlinear characteristics of the system, approximately transforming the nonlinear control problem into a linear control problem. A sliding mode controller which is insensitivity to parameter uncertainties and strong robustness to external disturbance is designed based on the compensated model. Simulation results show that the proposed closed-loop control method can significantly improve the tracking accuracy of MRD.

Control strategy is significant for the performance of semi-active suspension.[22] Plenty of control algorithms have been proposed, for example, skyhook control[23] for suppressing sprung mass vibration, and groundhook control[24] to mitigate unsprung mass vibration. Since the ride comfort, handling stability and actuator saturation should be captured in the design of suspension system, a H_∞ control method considering both the performance and constraints is suggested for the active suspension,[25] but the controller is fixed, the performance of the system cannot be adjusted according to the road information. Subsequently, a moving horizon H_∞/generalized H_2 strategy is proposed to improve the performance while considering the worst-case uncertainties and disturbances.[26] However, the control problem is solved by linear matrix inequalities, and the obtained solution is always very conservative.[25,26] The limitations for suspension system can be listed as: one is the typically fast dynamics of the road excitations, the other is the time delay of the communication buses. In recent years, the development of radar, laser sensing and other technologies has enabled road preview technology to be implemented.[27] The existing work[28] has shown that the effects listed above can be significantly improved by road preview control, in which the road excitation is taken as a measured external input instead of an unknown disturbance. With road preview technology, the road excitation can be purposefully compensated by appropriate control algorithm.[29] A review of suspension controllers with road preview is proposed,[30] which emphasized that the vehicle performance can be further improved with preview. Meanwhile, it's pointed out that based on characteristics of predicting the future behavior of the system, and the capability of directly considering constraints, model predictive control (MPC) is the preferred control structure for the implementation of road preview. An incremental MPC strategy is studied for active suspension based on the information of the preceding vehicle,[31] however, the system constraints are not considered. Subsequently, based on global road information, a hybrid time-varying preview MPC strategy for semi-active suspension is proposed.[32] To reduce the computational load of traditional MPC, an explicit MPC method is suggested.[33] All requirements are weighted and expressed into a single cost function to tradeoff conflicting requirements, and an optimal controller is obtained by minimizing the cost function.[32,33] But for specific problems, it's difficult to choose suitable weighting matrices, which leads to the driving safety cannot be guaranteed in some conditions. Moreover, the constrains should be within given bounds rather than to be minimized.[25] Therefore, taking all the different requirements in a single objective function and minimizing it may lead to conservative. To further optimize the performance of the semi-active suspension, a preview MPC scheme is proposed in this article to achieve the best possible ride comfort while ensuring driving safety.

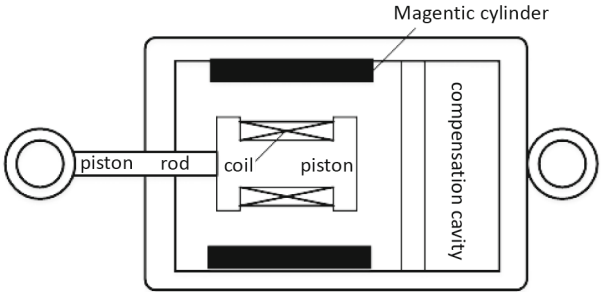

FIGURE 1 The structural of MRD.

In order to improve the comprehensive performance of vehicle suspension, a road preview model predictive controller is designed in this article, which takes the road excitation as a measurable disturbance, the sprung mass acceleration as the cost function, and the suspension stroke, tire deformation and actuator saturation as constraints. Simulation results for a quarter-car suspension show that compared with the H_∞/generalized H_2 control strategy,[26] the road preview MPC scheme can effectively tradeoff constraints satisfaction and performance improvement.

The remainder of this article is as follows. In Section 2, the experimental setup used for analysing the dynamics of MRD is presented and the identification of the Hammerstein model is discussed. Controller design methods for MRD and semi-active suspension are expressed in Sections 3 and 4, respectively. Simulation results are carried out in Section 5. The article is ended by some concluding remarks.

2 | MAGNETO-RHEOLOGICAL DAMPER

To evaluate the application of MRD for vehicle suspension system, experiments are set up to get its dynamic data, and a Hammerstein model is designed to accurately characterize the dynamics of MRD using the obtained experimental data. Finally, simulation results are given to verify the effectiveness of the Hammerstein model.

2.1 | Dynamics of MRD

The structure of MRD is shown in Figure 1. The core components are piston, rod, coil, magnetic cylinder, compensation cavity, and magnetorheological fluid. The damping force of MRD is directly related to the magnetic field strength and the current in the coil.

The MRD is tested with different currents and piston velocities. The experimental data for the MRD characteristics is measured on the MTS850 testbed based on the test method QC/T545-1999 of automotive shock absorber. The test amplitude s for MRD stroke is ± 20 mm. The piston velocity is set as $v_1 = 0.262$ m/s, $v_2 = 0.524$ m/s. The control current I of the MRD is $0 \sim 1$ A. The tests for damping characteristics are shown in Figures 2–5.

Figures 2 and 4 show that at different piston velocities, the damping force increases with the current value in the coil. Figures 3 and 5 reflect that the damping force of the MRD exhibits obvious hysteresis characteristics with the change of piston velocities, and the hysteresis loop becomes larger with the increase of the current value. When the piston velocity is selected as v_1, the damper force is within $[-1900N, 1600N]$, while as v_2, the upper and lower limits of the damper force are $2500N$ and $-2500N$, respectively.

2.2 | Modeling of MRD

In order to accurately track the expected damping force, a Hammerstein model has been constructed in this section, which consists of a static nonlinear block, and a linear dynamic block as shown in Figure 6.

Neural network has the capability to approximate arbitrary nonlinear functions with arbitrary accuracy.[34] Therefore, a double hidden layer BP neural network is used to identify the static nonlinear block of the Hammerstein model: current I, piston displacement s and the piston velocity v are selected as the inputs, the output is the predicted damping force F_{d0}.

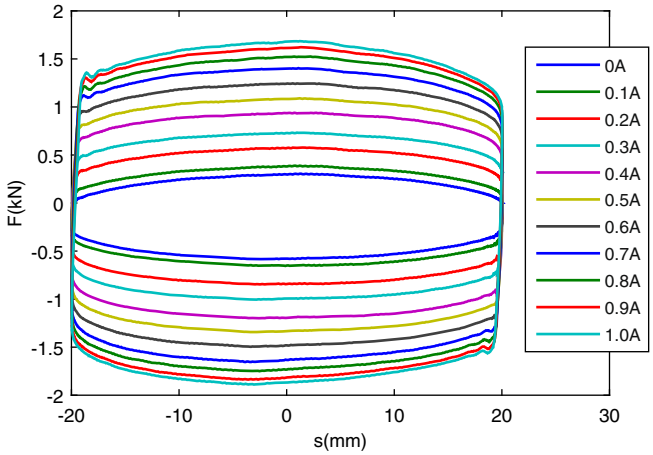

FIGURE 2 The curve of damping force F_d and piston displacement s.

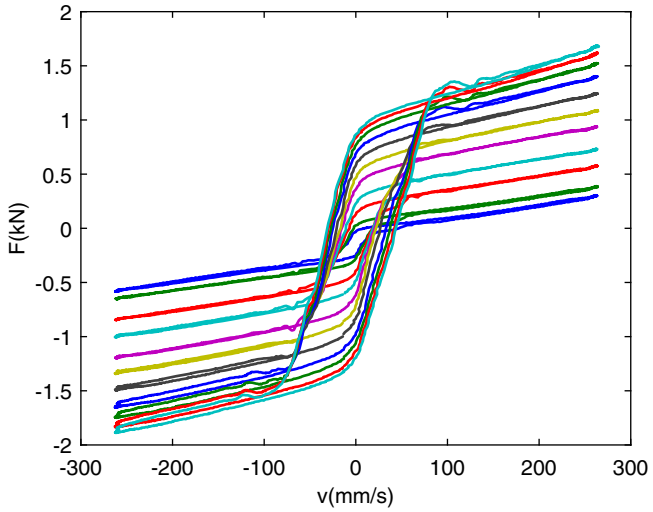

FIGURE 3 The curve of damping force F_d and piston velocity v_1.

Taking the tansig function as the transfer function of hidden layer neurons, and the purelin function as the transfer function of output layer neurons, the model of the static nonlinear block is established. Levenberg–Marquardt algorithm[35] is applied to adjust the unknown parameters to make the root mean squared error (RMSE) between the output of the neural network model and the experiment data obtained by the MTS850 testbed within 10^{-3}. The number of neurons in double hidden layers is 12. When the piston velocity is chosen as $v_1 = 0.262$ m/s, piston displacement s is 20 mm, control current I is $0 \sim 1$ A, the neural network training results are as follows:

Figures 7 and 8 show that the output damping force of the neural network model is basically consistent with the output of the testbed, and can well approximate the damping characteristics of MRD. The RMSE between the output of the neural network model and the experiment data is 0.00069. Therefore, the obtained BP neural network can be used to establish the static nonlinearity model of MRD.

However, BP neural networks are essentially a class of static nonlinear mappings. To accurately characterize the hysteresis of MRD, dynamic properties need to be considered. The least square method is used to identify the transfer function between the output damping force F_{d0} of the direct neural network model and the actual damping force F_d:

$$G(s) = \frac{579800}{s^2 + 671.5s + 579900}, \tag{1}$$

The two poles of $G(s)$ are $-335.75 + 683.5i, -335.75 - 683.5i$, which are all on the left half plane, and indicate that the identified transfer function is stable.

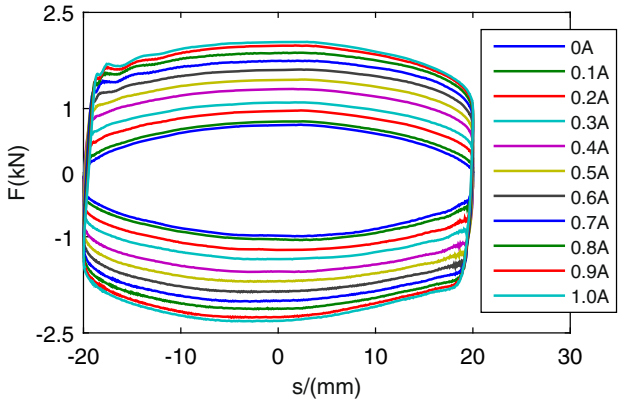

FIGURE 4 The curve of damping force F_d and piston displacement s.

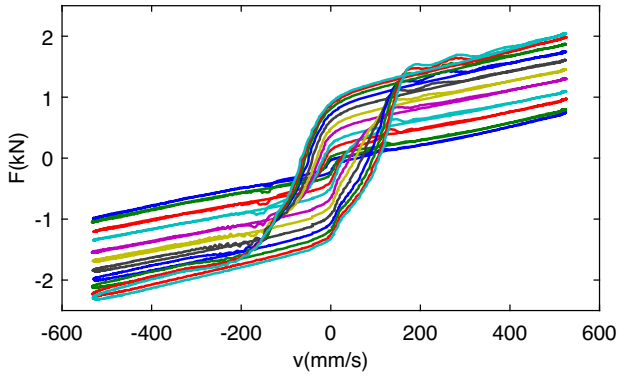

FIGURE 5 The curve of damping force F_d and piston velocity v_2.

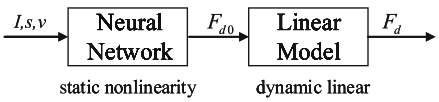

FIGURE 6 The structure of Hammerstein model.

The step response and Bode diagram of $G(s)$ are shown in Figures 9 and 10 respectively.

Figure 9 shows that the system has a short setting time and a relative-high overshoot. Figure 10 shows the Bode diagram of $G(s)$. The low-frequency (less than 100 Hz) signal will pass $G(s)$ without magnitude attenuation and phase delay. Therefore, $G(s)$ is robust to low-frequency signal. But for high-frequency signal, a controller is needed to improve its robustness.

Transform $G(s)$ in (1) into its state space form:

$$\begin{cases} \dot{z} = Az + BF_{d0} \\ F_d = Cz, \end{cases} \tag{2}$$

where

$$z = \begin{bmatrix} z_1 & z_2 \end{bmatrix}^T \in \Re^{2\times 1}, A = \begin{bmatrix} a_{11} & a_{12} \\ a_{21} & a_{22} \end{bmatrix} = \begin{bmatrix} 0 & 1 \\ -579900 & -671.5 \end{bmatrix},$$
$$B = \begin{bmatrix} b_{11} & b_{21} \end{bmatrix}^T = \begin{bmatrix} 0 & 1 \end{bmatrix}^T, C = \begin{bmatrix} c_{11} & c_{c_{12}} \end{bmatrix} = \begin{bmatrix} 579800 & 0 \end{bmatrix},$$

input F_{d0} is the damping force generated by the static nonlinear sector, F_d is the actual output of MRD.

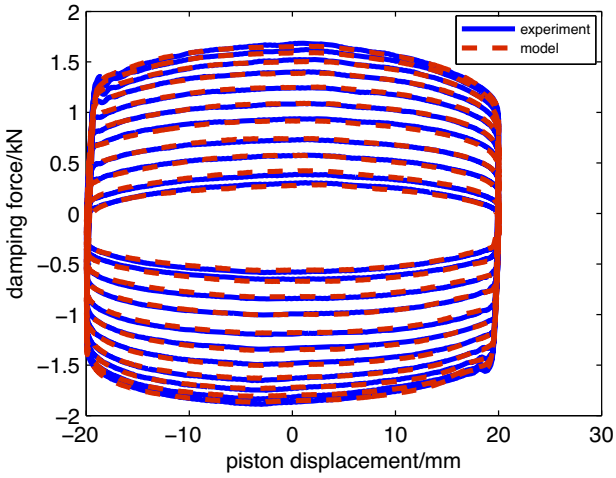

FIGURE 7 The curve of damping force F_{d0} and the piston displacement s.

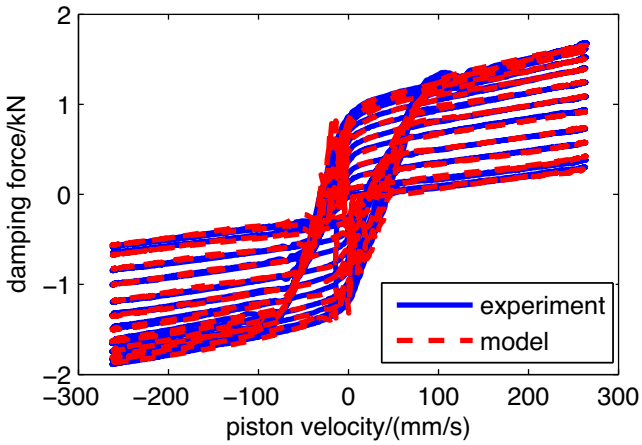

FIGURE 8 The curve of damping force F_{d0} and the piston velocity v_1.

Remark 1. z_1 and z_2 are the states of $G(s)$, which have no physical meaning.

2.3 | Model verification and validation

When the damper piston velocity is chosen as $v_2 = 0.524$ m/s, piston displacement s is 20 mm, control current I is $0 \sim 1$ A, the output damping force of the static model and Hammerstein model is shown in Figure 11, the RMSE between the predicted and actual output is used to evaluate the performance of the static model and Hammerstein model.

Figure 11 shows that the damping force is distributed in $[-2500N, 2500N]$. The RMSE of the static model and Hammerstein model is 0.0243 and 0.0058, respectively. It can be seen from the comparison of the error curves in Figure 12 that the Hammerstein model can reduce the modeling error.

3 | CONTROL OF MRD

In order to make the MRD quickly and effectively track the desired damping force, a sliding mode controller connected with a neural network inverse model has been designed as the lower-level controller. The control structure is shown in Figure 13.

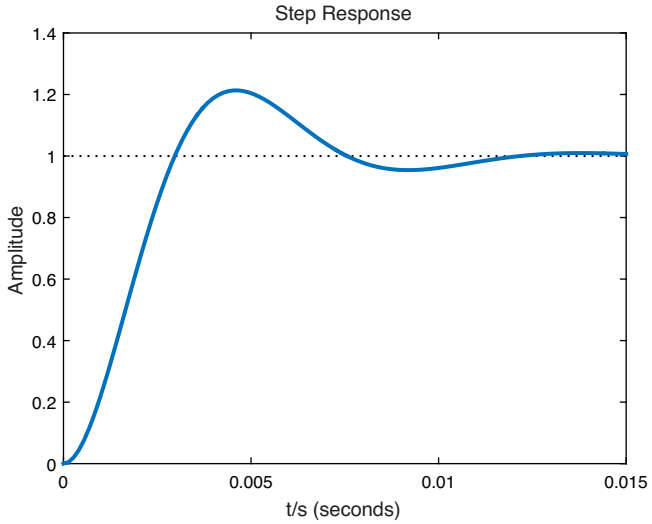

FIGURE 9 Step response of $G(s)$.

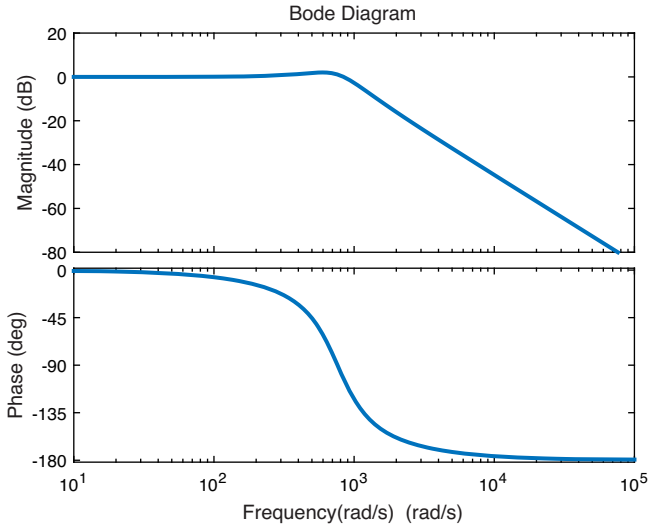

FIGURE 10 Bode diagram of $G(s)$.

3.1 | Inverse neural network

The neural network inverse model is mainly used to generate a current to drive MRD. Here, double hidden layer BP neural network is used to identify the inverse model of MRD. As shown in Figure 14, F_d, piston displacement s, and piston velocity v are selected as the input variables of the neural network, the output of the neural network is current I. Both of the numbers of two hidden layer neurons are 12. The transfer function and training function are selected the same as the direct neural network.

Take the piston velocity $v_2 = 0.524$ m/s to verify the accuracy of the inverse model. The error curve is shown in Figure 15, in which spikes appear at individual points due to piston commutation or current switching within the acceptable range. Therefore, the established inverse model of MRD can accurately calculate the excitation current in real time, and can be used for real-time control of semi-active suspension.

The neural network inverse model can be used to compensate its nonlinear part of MRD, resulting in linear or approximately linear characteristics.

The compensation results are shown in Figure 16, in which the RMSE is 0.0292, indicating that the nonlinear part of the Hammerstein model can be compensated by the neural network inverse model, but with a compensation error.

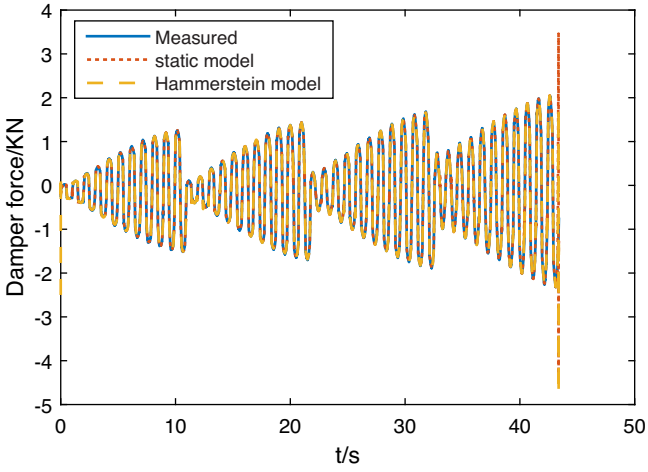

FIGURE 11 Damper force.

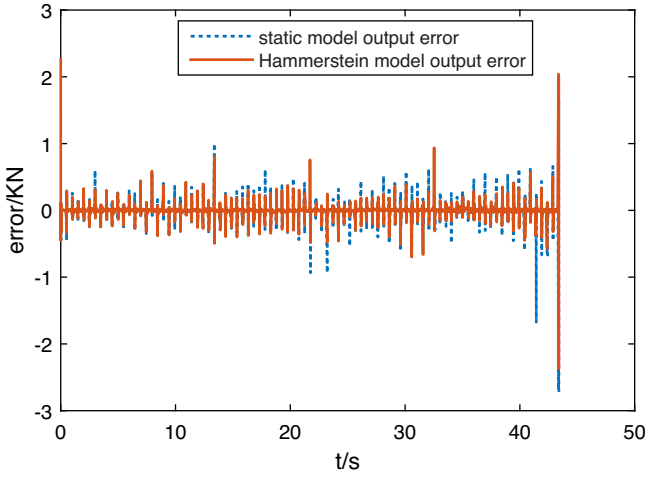

FIGURE 12 Damper force error.

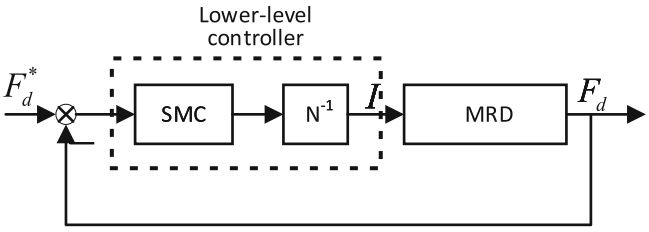

FIGURE 13 Control structure of MRD.

3.2 | Sliding mode control of MRD

The damping force of MRD is strongly dependent on temperature changes, that is, heat generation caused by friction in the operation of MRD leads to modeling parameter mismatch. Thus the control effect will be seriously reduced. Since sliding mode controller is insensitive to parameter uncertainties and external disturbance, it is designed to deal with modeling uncertainties or compensation errors.

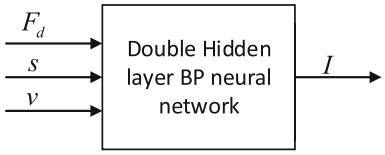

FIGURE 14 The inverse model of MRD.

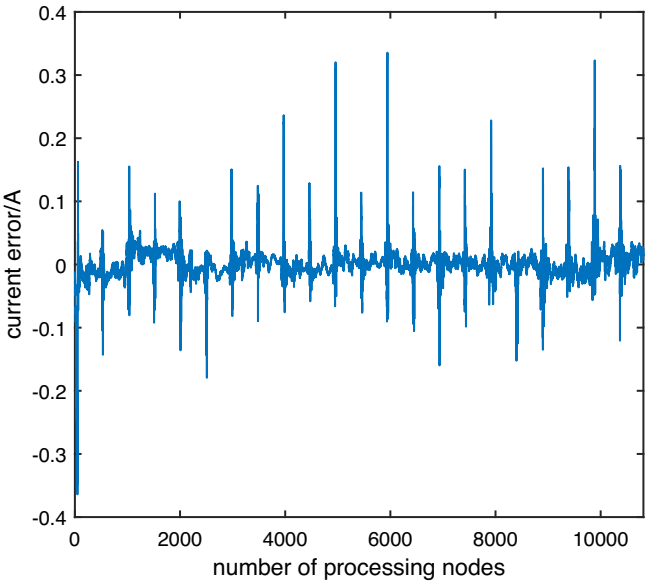

FIGURE 15 Training error versus number of processing nodes in the network.

Select sliding mode surface ζ as

$$\zeta = ce + \dot{e}, \tag{3}$$

in which

$$e = F_d^* - F_d. \tag{4}$$

Its first-order and second-order derivative are

$$\begin{aligned} \dot{e} &= \dot{F}_d^* - \dot{F}_d \\ \ddot{e} &= \ddot{F}_d^* - \ddot{F}_d, \end{aligned} \tag{5}$$

respectively, where $c \in \Re^1$ is a constant, F_d^* the reference input.

The derivative of (3) is

$$\begin{aligned} \dot{\zeta} &= c\dot{e} + \ddot{e} \\ &= c\left(\dot{F}_d^* - \dot{F}_d\right) + \ddot{F}_d^* - \ddot{F}_d. \end{aligned} \tag{6}$$

In terms of (2), $\dot{F}_d = c_{11}\dot{z}_1$, $\ddot{F}_d = c_{11}\ddot{z}_1$, $\dot{z}_1 = z_2$ and $\dot{z}_2 = a_{21}z_1 + a_{22}z_2 + h$. Thus,

$$\dot{\zeta} = c\dot{F}_d^* - cc_{11}z_2 + \ddot{F}_d^* - c_{11}\left(a_{21}z_1 + a_{22}z_2 + h\right). \tag{7}$$

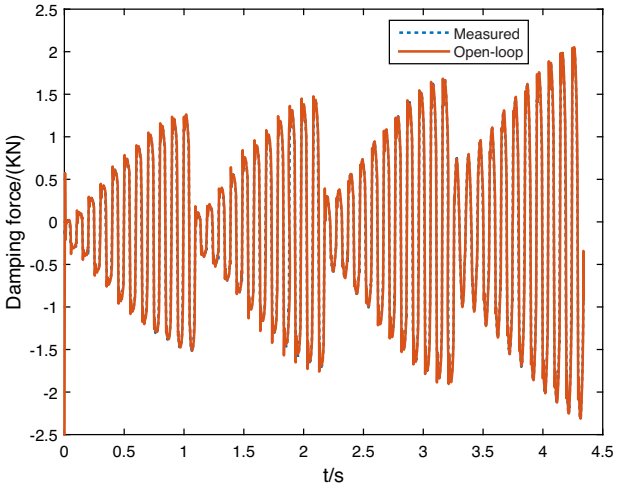

FIGURE 16 Compensation results of the static nonlinear sector by neural network inverse model.

Choose the exponential convergence principle as[36]

$$\dot{\zeta} = -\varepsilon sign(\zeta) - m\zeta, \tag{8}$$

where $sgn(\zeta)$ is the sign function of ζ, ε and m are related to the rate of convergence.

In accordance with (7) and (8), the control principle is

$$h = \frac{\ddot{F}_d^*}{c_{11}} + \frac{c}{c_{11}}\dot{F}_d^* - a_{21}z_1 - (cz_2 + a_{22}z_2) + \frac{\varepsilon sign(\zeta) + m\zeta}{c_{11}}. \tag{9}$$

Define a candidate Lyapunov function:

$$V = \frac{1}{2}\zeta^2. \tag{10}$$

Then,

$$\begin{aligned} \dot{V} &= \zeta\dot{\zeta} \\ &= \zeta(-\varepsilon sign(\zeta) - m\zeta) \\ &= -\varepsilon|\zeta| - m\zeta^2. \end{aligned} \tag{11}$$

If parameters ε and m are selected to be positive, the system states will converge to the sliding mode surface.

3.2.1 | Search for parameters c, ε, and m

Here, genetic algorithm (GA) is used to search the proper parameters of sliding mode controller. The selection of fitness function is significant for GA.[37]

Considering the upper layer adopts MPC, assumed that $F_d^*(k)$ is the expected damping force calculated by the model predictive controller in the k_{th} moment, then (2) should be discretized by using Euler method, that is,

$$\begin{cases} z(k+1) = \Theta z(k) + Gh(k) \\ F_d(k) = Cz(k), \end{cases} \tag{12}$$

where $\Theta = \Xi_1 + TA$, $G = TB$, Ξ_1 is an identity matrix with the same dimension as A, the sampling period $T = 0.01$ s.

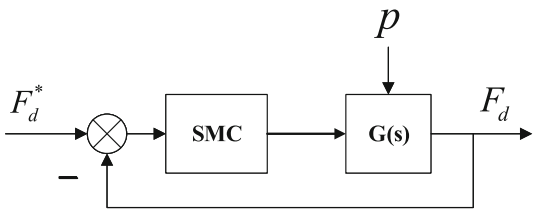

FIGURE 17 Control structure of MRD with compensated model.

The fitness function is chosen as

$$\sum_{k=1}^{n}\left(F_d^*(k) - F_d(k)\right)^2, \tag{13}$$

where $F_d(k)$ is the output in the kth moment, n is the simulation step size. The core of it is to minimize the variance between the output of the system and the given reference input within the sampling time. A reference signal is selected as

$$F_d^*(k) = 2.5\sin(2\pi k).$$

To avoid local minimum, select the initial population, iteration and fitness function as 150, 10,000, 10^{-10}, respectively. The determined parameters are $c = 1957.393$, $\varepsilon = 636.396$, and $m = 1946.978$.

Remark 2. In the operation of the actual system, both $\dot{F}_d^*$ and $\ddot{F}_d^*$ are unknown, which can be approximated by $\dot{F}_d^*(k-T)$ and $\ddot{F}_d^*(k-T)$ since F_d^* is smooth in general.

3.3 | Simulation results of sliding mode controller

Simulation experiments are carried out on MRD to verify the effectiveness of the sliding mode controller. The reference signal is selected as

$$y^* = 2.5\sin(2\pi ft)$$

According to the working frequency of MRD, frequency f is chosen as 1 and 2.5 Hz respectively.

In order to test the robustness of the controller, a white Gaussian noise signal with a mean of 0 and a variance of 0.03 is added as lumped disturbances (compensated error, modeling error, measurement noise, etc.), as shown in Figure 17.

The experimental results in Figures 18–21 show that compared with open-loop control, sliding mode control can make MRD track the reference damping force quickly and accurately.

4 | CONTROL OF SUSPENSIONS

The control objective is to minimize the sprung mass acceleration, while respecting good handling and keeping suspension strokes within bounds. Moreover, damper forces, generated by MRD, should be bounded because of actuator saturation. A hierarchical control strategy is adopted, which is shown in Figure 22. The upper-layer is based on road preview MPC method to obtain the desired damper force F_d^*. The lower layer uses a sliding mode controller in series with the neural network inverse model designed in Figure 13 to make the output damping force of MRD (F_d) accurately track the expected damping force (F_d^*).

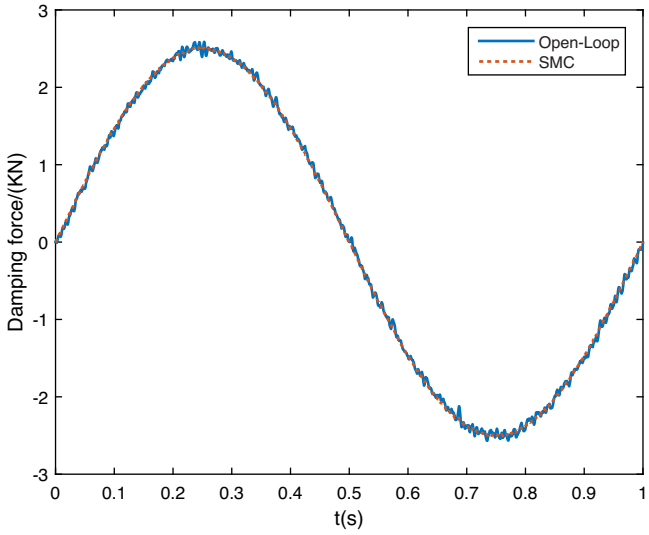

FIGURE 18 Desired damping force tracking curve ($f = 1$ Hz).

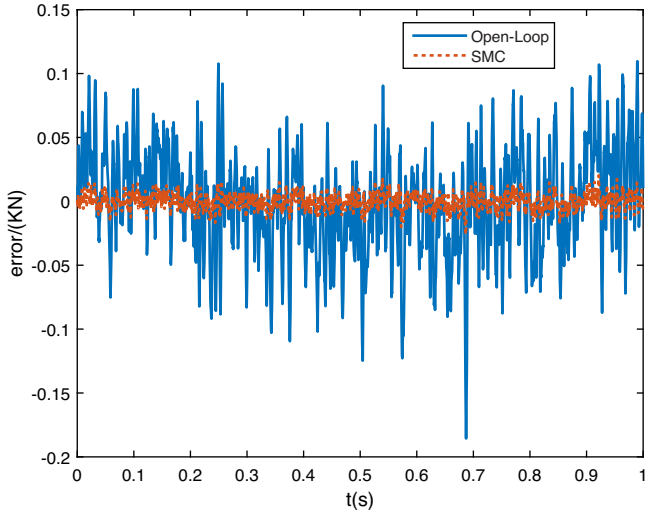

FIGURE 19 Desired damping force tracking error curve ($f = 1$ Hz).

4.1 | Modeling of semi-active suspension

A quarter-car semi-active suspension model with a preview sensor is shown in Figure 23.[38]

The two-degree-of-freedom model of the quarter-car semi-active suspension is:

$$\begin{cases} m_s\ddot{x}_s + c\left(\dot{x}_s - \dot{x}_u\right) + k_s\left(x_s - x_u\right) = F_d \\ m_u\ddot{x}_u + c\left(\dot{x}_u - \dot{x}_s\right) + k_s\left(x_u - x_s\right) + k_t\left(x_u - x_r\right) = -F_d, \end{cases} \tag{14}$$

where x_s and x_u represent the displacement of the sprung mass and unsprung mass respectively, m_s is the sprung mass, m_u is unsprung mass, k_s denotes the suspension spring stiffness, c is the uncontrollable damping coefficient, and k_t is the tire stiffness. The road displacement is expressed as x_r.

Choose the state x as $[x_s - x_u, \dot{x}_s, x_u - x_r, \dot{x}_u]^T$, and establish the state-space equation of the semi-active suspension:

$$\dot{x} = A_c x + B_{cu} u + B_{cd} d, \tag{15}$$

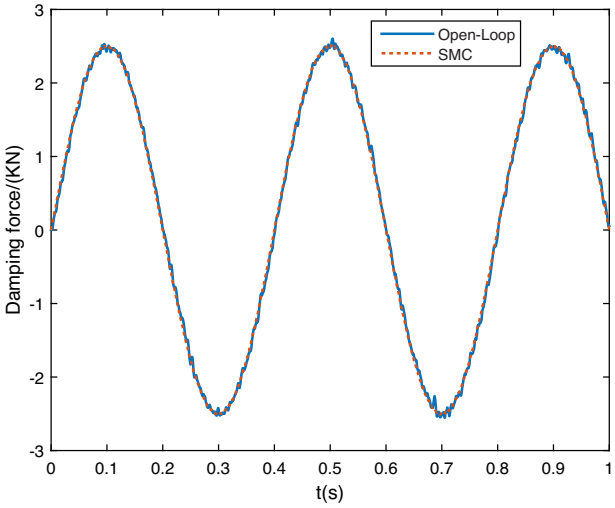

FIGURE 20 Desired damping force tracking curve ($f = 2.5$ Hz).

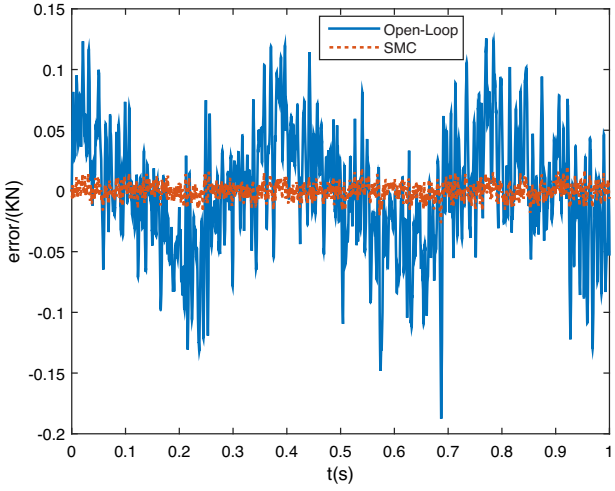

FIGURE 21 Desired damping force tracking error curve ($f = 2.5$ Hz).

where u and d represent F_d and $\dot{x}_r$ respectively,

$$A_c = \begin{bmatrix} 0 & 1 & 0 & -1 \\ -\frac{k_s}{m_s} & -\frac{c}{m_s} & 0 & \frac{c}{m_s} \\ 0 & 0 & 0 & 1 \\ \frac{k_s}{m_u} & \frac{c}{m_u} & -\frac{k_t}{m_u} & -\frac{c}{m_u} \end{bmatrix}, \quad B_{cu} = \begin{bmatrix} 0 & \frac{1}{m_s} & 0 & -\frac{1}{m_u} \end{bmatrix}^T, \quad B_{cd} = \begin{bmatrix} 0 & 0 & -1 & 0 \end{bmatrix}^T.$$

Remark 3. In look-ahead preview control, it is assumed that the road displacement x_r in front of the vehicle, and its changing rate $\dot{x}_r$ can be measured by sensors.[38]

The constraints include:[25]

(1) Good road holding requires the dynamic tire load should be less than the static ones, which is equivalent to

$$k_t (x_u - x_r) < f_{ku}, \tag{16}$$

where f_{ku} is the static tire load, and $f_{ku} = (m_s + m_u) g$.

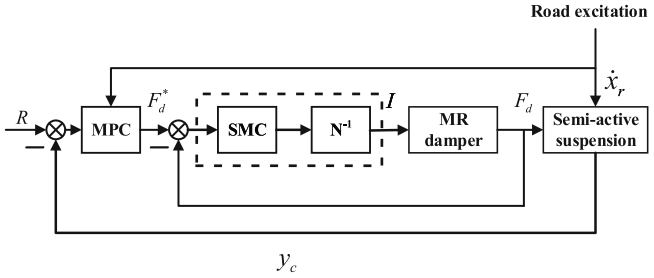

FIGURE 22 The overall control block diagram.

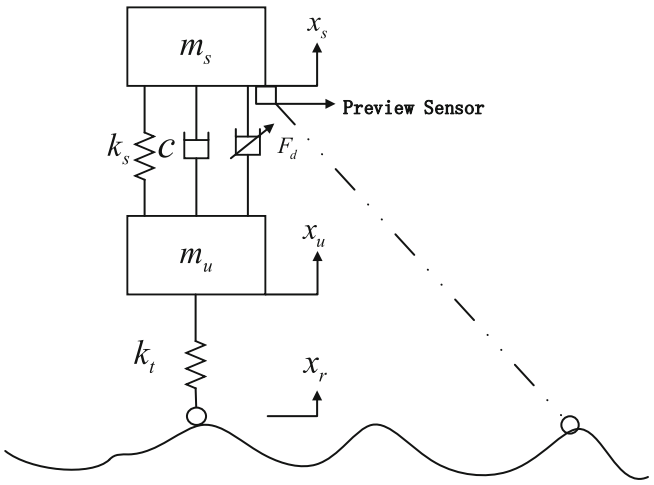

FIGURE 23 A quarter-car semi-active suspension model with preview sensor.

(2) Due to the mechanical structure of suspension, the dynamic stroke of the suspension should also be limited to a given range to avoid excessive suspension bottoming, which will result in structural damage,

$$|x_s - x_u| \leq S_{\max}, \tag{17}$$

where $S_{\max} > 0$ is the largest suspension stroke.

(3) Considering the output saturation of the actuator, the control variable should satisfy

$$|F_d| \leq F_{d\max}, \tag{18}$$

where $F_{d\max}$ is the largest damper force.

4.2 | Model predictive controller

The controller design objective is to minimize the sprung mass acceleration $\ddot{x}_s$ to achieve the best possible ride comfort while satisfying the constraints in Equations (16)–(18).

Discretize (15) by using Euler method:

$$x(k+1) = \Phi x(k) + Hu(k) + Jd(k), \tag{19}$$

where $\Phi = \Xi_2 + TA_c$, $H = TB_{cu}$, $J = TB_{cd}$, Ξ_2 is an identity matrix with the same dimension as A_c, the sampling period $T = 0.01$ s.

According to the requirements mentioned above, denote the sprung mass acceleration $\ddot{x}_s$ as the control output y_c, the suspension stroke $x_s - x_u$ and the tire dynamic deflection $x_u - x_r$ as the constraint outputs y_b, which can be represented in discrete time as

$$\begin{aligned} y_c(k) &= C_c x(k) + D_c u(k), \\ y_b(k) &= C_b x(k), \end{aligned} \tag{20}$$

where

$$C_c = \begin{bmatrix} -\frac{k_s}{m_s} & -\frac{c}{m_s} & 0 & \frac{c}{m_s} \end{bmatrix}, C_b = \begin{bmatrix} 1 & 0 & 0 & 0 \\ 0 & 0 & 1 & 0 \end{bmatrix}, D_c = \frac{1}{m_s}.$$

The cost function of the optimization problem is defined as:

$$J = \sum_{i=1}^{p} \|y_c(k+i|k)\|_Q^2 + \|u(k+i|k)\|_R^2, \tag{21}$$

where $k+i|k$ is the predicted value at time instant $k+i$ starting from time instant k, p is denoted as the prediction/control horizon, Q and R are positive definite weight matrices. The term $\|u(k+i|k)\|_R^2$ is to punish power consumption of actuator.

Problem 1:

$$\underset{U(k)}{\text{minimize}} \quad J\left(x\left(k\right), U\left(k\right)\right), \tag{22}$$

s.t.

$$\begin{aligned} & x\left(k+i+1|\,k\right) = \Phi x\left(k+i|\,k\right) + Hu\left(k+i|\,k\right) + Jd\left(k+i|\,k\right) \\ & y_c\left(k+i|\,k\right) = C_c x\left(k+i|\,k\right) + D_c u\left(k+i|\,k\right) \\ & y_b\left(k+i|\,k\right) = C_b x\left(k+i|\,k\right) \\ & |u(k+i|\,k)| \le F_{d\max}, i = 1, 2\cdots, p-1 \\ & |y_b(k+i|\,k)| \le y_{\max}, i = 1, 2\cdots, p, \end{aligned} \tag{23}$$

where

$$U\left(k\right) = \begin{bmatrix} F_d^*(k|k) & F_d^*(k+1|k) & \cdots & F_d^*(k+p|k) \end{bmatrix}^T, \tag{24}$$

and $\|y_b(k+i|k)\| \le y_{\max}$ is component-wise, that is,

$$y_{\max} = \begin{bmatrix} S_{\max} & f_{ku}/k_t \end{bmatrix}^T.$$

Problem 1 is a quadratic programming problem.[39,40] Only the first element of the "optimal" solution $F_d^*(k)$ will be applied to the system.

Remark 4. Preview scheme significantly improves ride comfort, especially in the first resonance frequency of the vehicle body, and a slight improvement in the secondary ride frequency range.[30] But the disadvantage of look-ahead preview is that inaccurate road information could be obtained. For example, for the road excitation which cannot be measured by preview sensor, like a water-filled pothole, disturbance d is defaulted as 0, while a bunch of leaves may be misinterpreted as an irregular road.

5 | ANALYSIS OF SIMULATION RESULTS

In this section, the performance of the proposed scheme applied to semi-active suspension with MRD is evaluated.

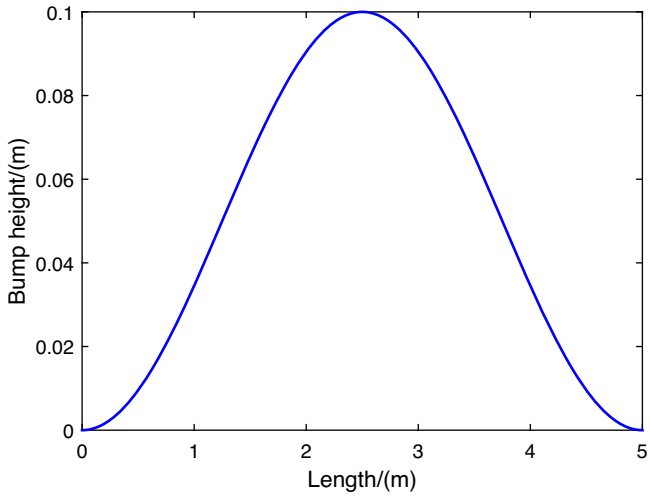

FIGURE 24 The curve of bump road.

TABLE 1 Parameters of quarter car semi-active suspension model.

m_s (kg)	m_u (kg)	k_s (N/m)	k_t (N/m)
320	40	22,000	180,000
c (N s/m)	$F_{d\max}$ (N)	$S_{\max}$ (m)	
1000	2500	0.08	

5.1 | Preview MPC of semi-active suspension with MRD

In this section, the proposed preview model predictive controller is applied to the quarter-car semi-active suspension mentioned above. C-grade road surface and bump roads are adopted to verify its effectiveness.

5.1.1 | Vibration isolation performance with bump roads

Bump roads seriously affect handling stability and ride comfort of vehicles. In this article, the preview length is taken as 18 m, and a bump is set 18 m away from the origin. The bump shown in Figure 24 is described as follows[25]

$$x_r = \begin{cases} \frac{A}{2}\left(1 - \cos\frac{2\pi V(t-t_0)}{L}\right), & t_0 \le t \le \frac{L}{V} + t_0 \\ 0, & \text{otherwise} \end{cases} \tag{25}$$

with height $A = 0.1$ m and length $L = 5$ m, t_0 is the time when the vehicle enters the bump. Assume that the speed of vehicle V remains constant when passing the bump.

Parameters of quarter-car semi-active suspension are in Table 1.

Choose the prediction/control horizon $p = 60$, weight matrices $Q = 1.5$, $R = 0.0008$.

When the vehicle passes the bump with $V = 10$ m/s, compared with the H_∞/generalized H_2 control scheme,[26] the evolution of sprung mass acceleration, suspension stroke, dynamic and static tire load ratio and damping force are shown in Figures 25–28. Both the H_∞/generalized H_2 scheme and the preview MPC algorithm satisfy constrains, and have similar performance. Additionally, it can be seen from Figure 25 that vehicle with H_∞/generalized H_2 control strategy or preview MPC strategy responses to the bump at 1.8 and 1.2 s, respectively. This is because the selected prediction/control horizon $p = 60$, and the sampling period $T = 0.01$ s, compared with the H_∞/generalized H_2 controller, the proposed preview model predictive controller will respond to the bump 0.6 s earlier, which reduces the ride comfort.

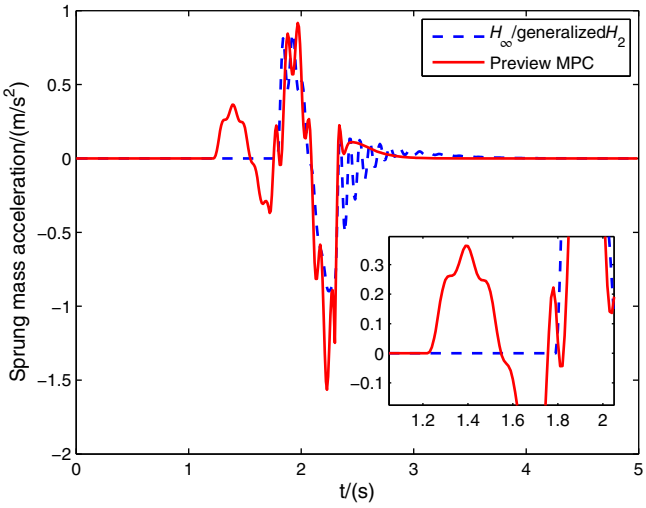

FIGURE 25 Sprung mass acceleration ($V = 10$ m/s).

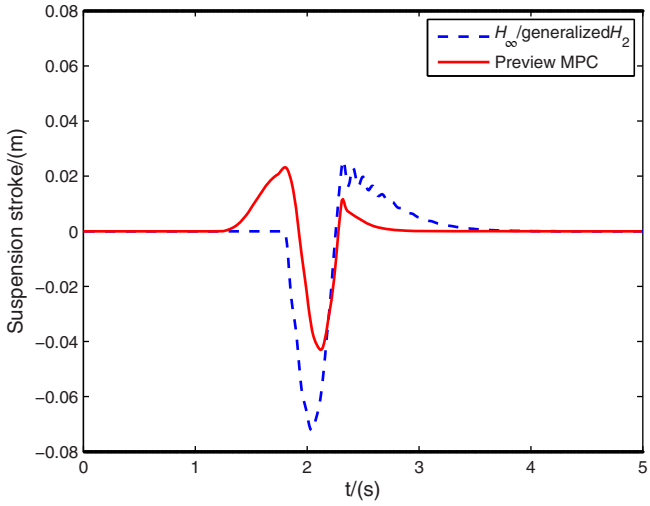

FIGURE 26 Suspension stroke ($V = 10$ m/s).

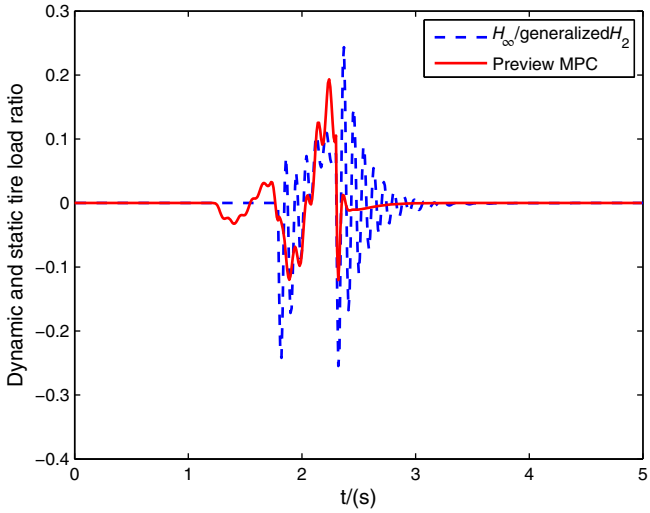

FIGURE 27 Dynamic and static tire load ratio ($V = 10$ m/s).

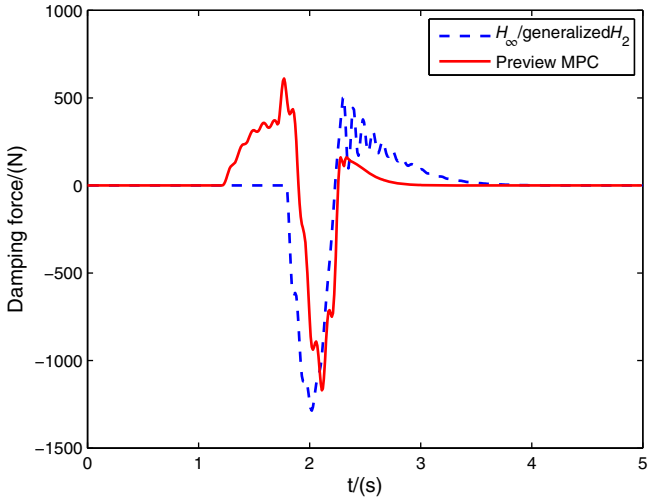

FIGURE 28 Damping force ($V = 10$ m/s).

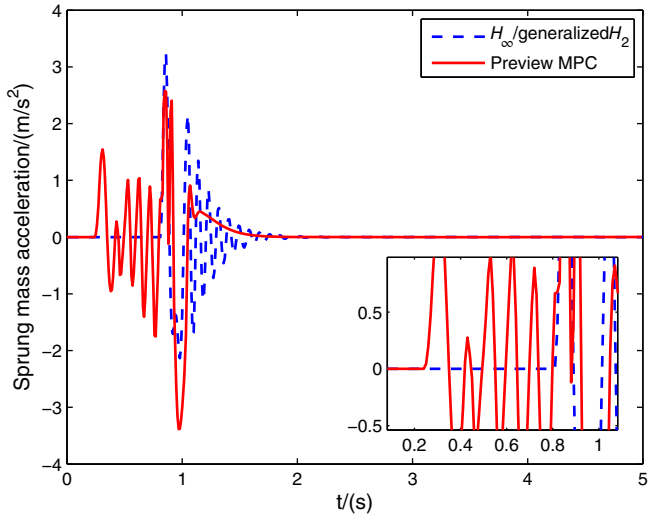

FIGURE 29 Sprung mass acceleration ($V = 22$ m/s).

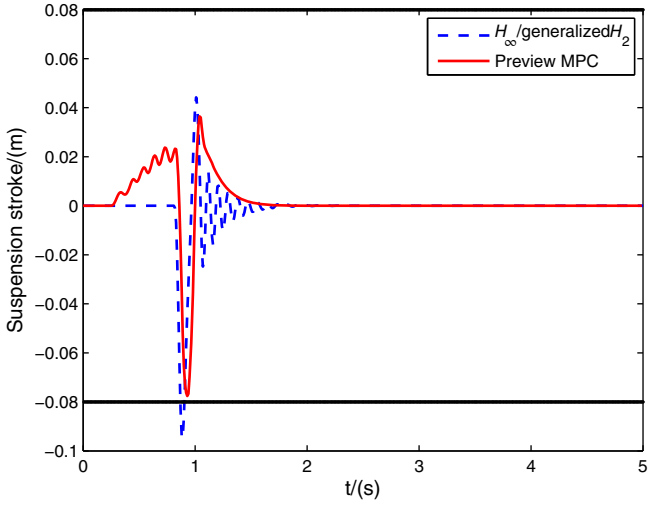

FIGURE 30 Suspension stroke ($V = 22$ m/s).

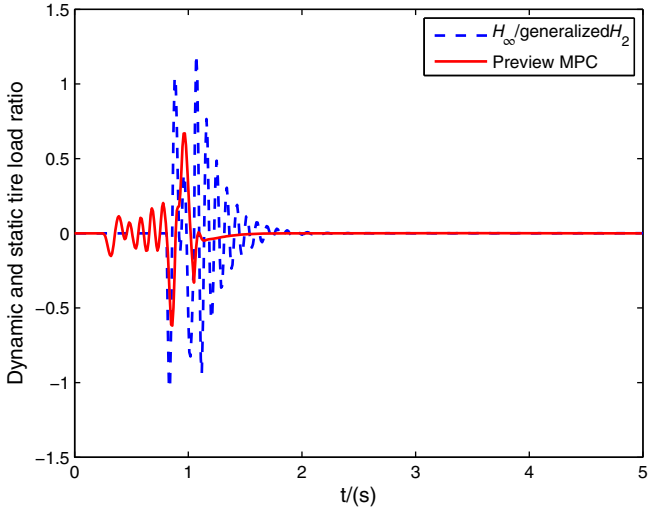

FIGURE 31 Dynamic and static tire load ratio ($V = 22$ m/s).

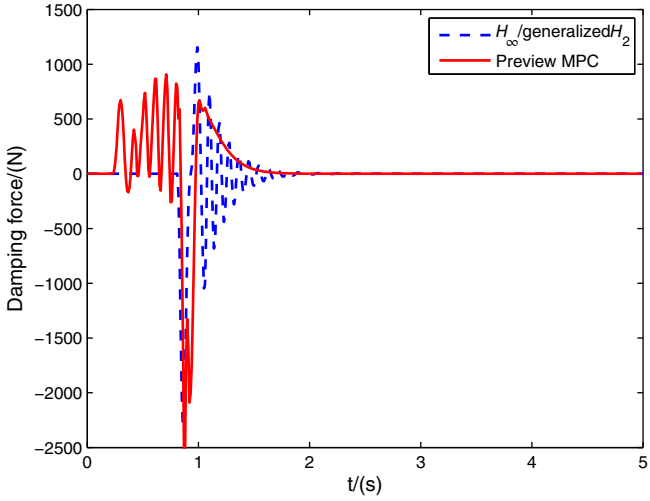

FIGURE 32 Damping force ($V = 22$ m/s).

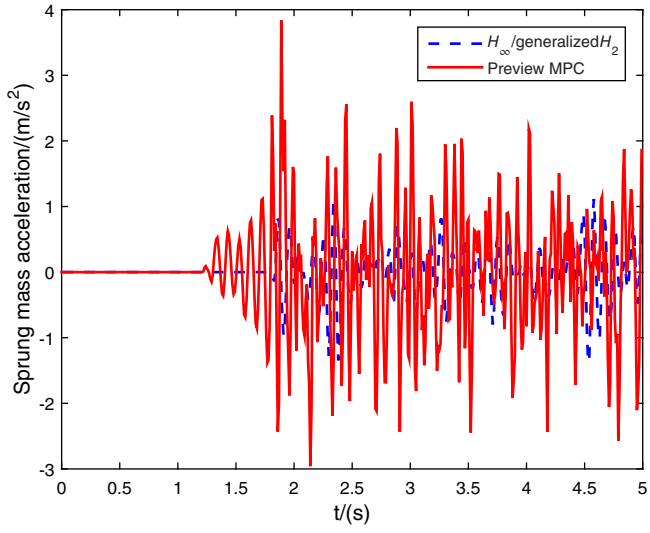

FIGURE 33 Sprung mass acceleration ($V = 10$ m/s).

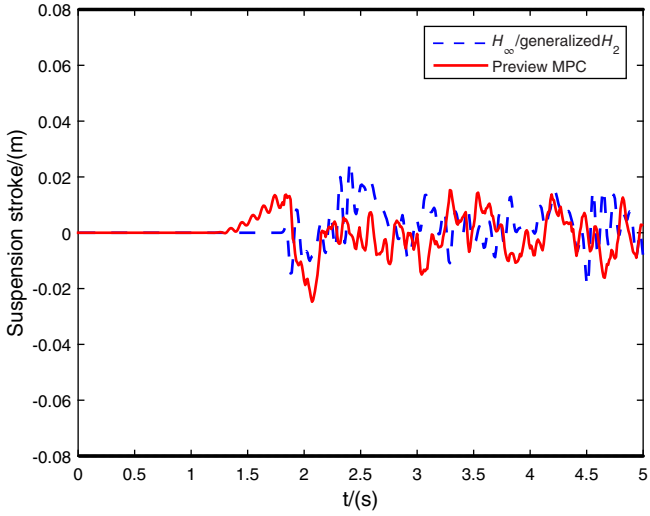

FIGURE 34 Suspension stroke ($V = 10$ m/s).

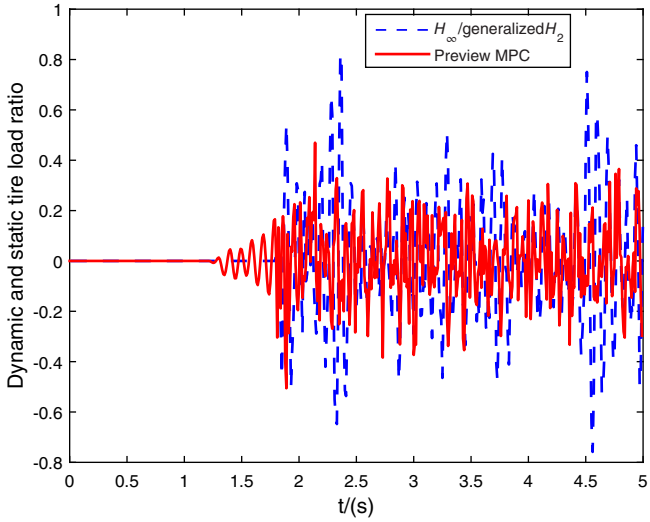

FIGURE 35 Dynamic and static tire load ratio ($V = 10$ m/s).

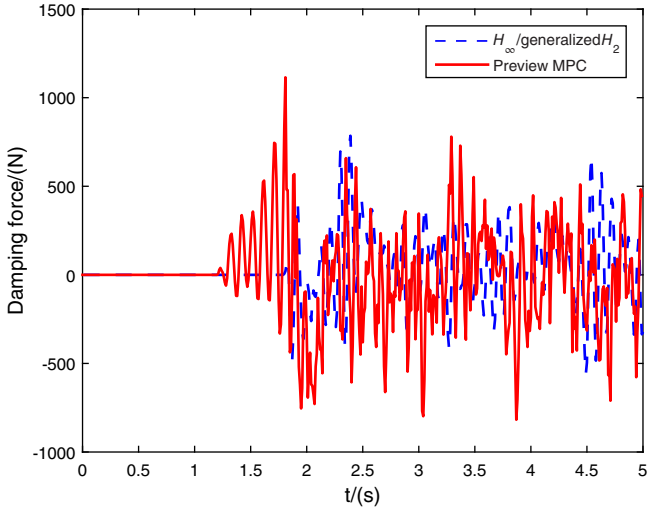

FIGURE 36 Damping force ($V = 10$ m/s).

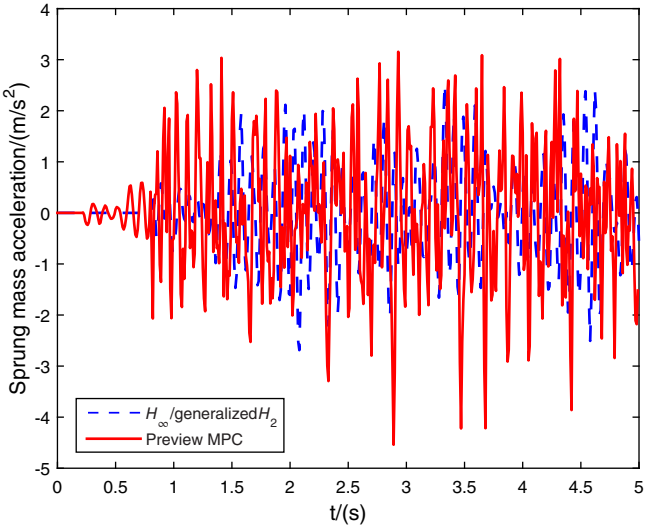

FIGURE 37 Sprung mass acceleration ($V = 22$ m/s).

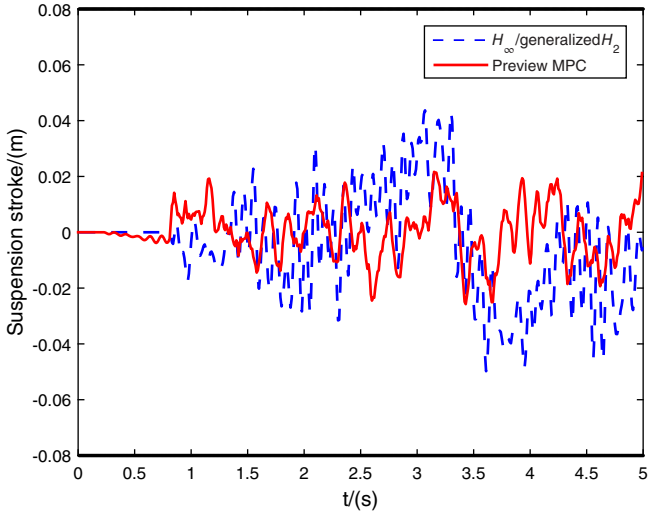

FIGURE 38 Suspension stroke ($V = 22$ m/s).

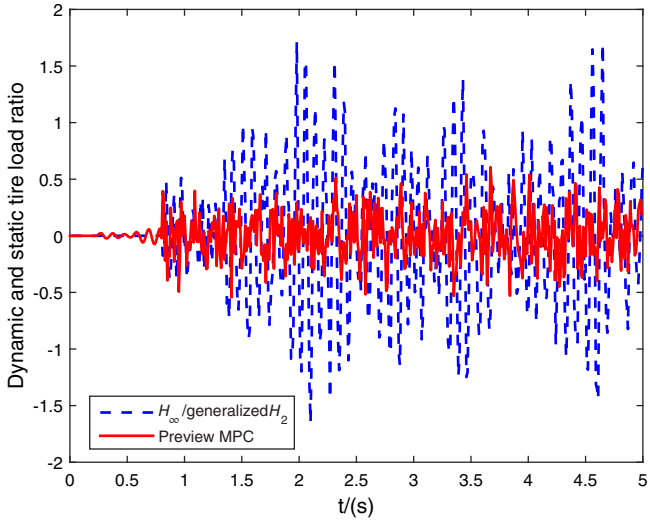

FIGURE 39 Dynamic and static tire load ratio ($V = 22$ m/s).

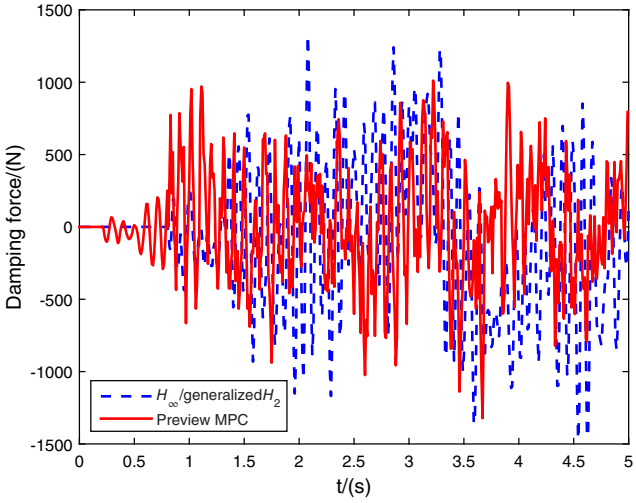

FIGURE 40 Damping force ($V = 22$ m/s).

When the vehicle speed increases to 22 m/s, as shown in Figures 29–32, the suspension stroke as well as the dynamic and static tire load ratio of the H_∞/generalized H_2 control scheme violate constraints while the preview MPC scheme still satisfies constraints. Figure 29 shows that the vehicle with H_∞/generalized H_2 control strategy and preview MPC strategy responses to the bump at 0.8 and 0.2 s, respectively, and with the preview MPC scheme, its sprung mass acceleration far exceeds that of the H_∞/generalized H_2 control scheme at 1 s, that is, the system constraints are satisfied at the cost of deterioration of system performance.

It can be found from the two scenarios ($v = 10$ m/s and $v = 22$ m/s), the vehicle will take action while it "detects" the bump from preview sensor, that is, the upcoming information permits vehicle to regulate conflict requirements in advance.

5.1.2 | Vibration isolation performance with C-grade road excitation

A C-grade road excitation is set 18 m away from the origin. When the speed of the vehicle is 10 m/s, compared with the H_∞/generalized H_2 control scheme, the evolution of sprung mass acceleration, suspension stroke, dynamic and static tire load ratio and damping force are shown in Figures 33–36.

Figures 33–36 shows that both the H_∞/generalized H_2 scheme and the preview MPC algorithm satisfy constrains, and the ride comfort improves effectively with H_∞/generalized H_2 control scheme.

When the vehicle speed increases to 22 m/s, the performance of the semi-active suspension is shown in Figures 37–40.

The dynamic and static tire load ratio of the H_∞/generalized H_2 control scheme violates constraints while the preview MPC scheme still satisfies constraints, and with the preview MPC scheme, its sprung mass acceleration far exceeds that of the H_∞/generalized H_2 control scheme, that is, the system constraints are satisfied at the cost of deterioration of system performance.

Therefore, it shows that for vehicles driving on both the bump roads and C-grade road excitation, the semi-active control suspension corresponding to the proposed control scheme sacrifices comfort, but the driving safety is significantly improved, that is, a balance between comfort and driving safety is achieved.

6 | CONCLUSION

Preview MPC of semi-active suspensions with MRD was proposed in this article. According to the strong nonlinearity and hysteresis characteristics of MRD, a Hammerstein model was established, and a cascade control method was designed accordingly. Simulation results showed that MRD with the cascade control scheme can significantly improve its tracking accuracy. Additionally, compared with H_∞/generalized H_2 control scheme, the proposed preview MPC scheme can maintain safety at the cost of reduction of ride comfort for semi-active suspensions.

ACKNOWLEDGMENTS

This work was supported by the National Natural Science Foundation of China under Grant U1964202.

CONFLICT OF INTEREST STATEMENT

The authors declare no potential conflict of interests.

DATA AVAILABILITY STATEMENT

Data sharing not applicable to this article as no datasets were generated or analyzed during the current study.

ORCID

Shuyou Yu https://orcid.org/0000-0002-3258-6494
Jie Guo https://orcid.org/0000-0002-3097-2412

REFERENCES

1. Chen H, Ma M, Sun P. Multi-objective control design for active suspensions: an LMI approach. *Acta Autom Sin*. 2006;10(4):550-559.
2. Nie S, Zhuang Y, Liu W, Chen F. A semi-active suspension control algorithm for vehicle comprehensive vertical dynamics performance. *Veh Syst Dyn*. 2017;55:1099-1122.
3. Nie S, Zhuang Y, Wang Y, Guo K. Velocity displacement-dependent damper: a novel passive shock absorber inspired by the semi-active control. *Mech Syst Signal Process*. 2018;99:730-746.
4. Savaia G, Formentin S, Panzani G, Corno M, Savaresi S. Enhancing skyhook for semi-active suspension control via machine learning. *IFAC J Syst Control*. 2021;17:100161.
5. Savaia G, Panzani G, Corno M, Sinigaglia A, Savaresi S. Tracking a reference damping force in a magneto-rheological damper for automotive applications. *IFAC-PapersOnLine*. 2020;53:14318-14323.
6. Carlson J, Joily M. MR fluid foam and elastomer devices. *Mechatronics*. 2000;10(4-5):555-569.
7. Phillips R. *Engineering Applications of Fluids with a Variable Yield Stress*. PhD Thesis. University of California, Berkeley; 1969.
8. GonZfilez A, Stiharu I, Sedaghati R. Practical hysteresis model for magneto-rheological dampers. *J Intell Mater Syst Struct*. 2014;25:967-979.
9. Ye M, Ang X. Parameter estimation of the Bouc-Wen hysteresis model using particle swarm optimization. *Smart Mater Struct*. 2007;26(6):2341-2349.
10. Wang E, Ma X, Rakhela S. Modelling the hysteretic characteristics of a magneto-rheological fluid damper. *Proc Inst Mech Eng D J Automob Eng*. 2003;217:537-550.
11. Stanway R, Sproston J, El-Wahed A. Applications of electro-rheological fluids in vibration control: a survey. *Smart Mater Struct*. 1996;5(4):464-482.
12. Wang D, Liao W. Semi-active controllers for magnetorheological fluid dampers. *J Intell Mater Syst Struct*. 2005;16:983-993.
13. Savaresi S, Bittanti S, Montiglio M. Identification of semi-physical and black-box non-linear models: the case of MR-dampers for vehicles control. *Automatica*. 2005;41(1):113-127.
14. Choi S, Lee S, Park Y. A hysteresis model for the field-dependent damping force of a magnetorheological damper. *J Sound Vib*. 2001;245(2):375-383.
15. Kim K, Lee C, Koo J. Design and modeling of semi-active squeeze film dampers using magneto-rheological fluids. *Smart Mater Struct*. 2008;17(3):135-141.
16. Sharma R, Gaur P, Bhatt S, Joshi D. Performance assessment of fuzzy logic control approach for MR damper based-transfemoral prosthetic leg. *IEEE Trans Artif Intell*. 2021;3:53-66.
17. Phu D, Tu P. A new adaptive fuzzy neural networks control using Riccati-like equation for controlling of magnetorheological fluid device. Proceedings of the 2020 6th International Conference on Control, Automation and Robotics (ICCAR); 2020:277-281.
18. Wang Z, Qin Y, Hu C, Dong M, Li F. Fuzzy observer-based prescribed performance control of vehicle roll behavior via controllable damper. *IEEE Access*. 2019;7:19471-19487.
19. Savaia G, Panzani G, Corno M, Cecconi J, Savaresi S. Hammerstein-Wiener modelling of a magneto-rheological dampers considering the magnetization dynamics. *Control Eng Pract*. 2021;112:104829.
20. Wei S, Wang J, Ou J. Experimental study on inverse model-based force tracking control of MR damper. *Shock Vib*. 2020;2020:1-14.
21. Yu S, Xu M, Sun X, Qu T, Zhuang Y, Chen H. Model predictive control of magneto-rheological damper semi-active suspension with preview. Proceedings of the 2020 Chinese Automation Congress (CAC); 2020:2755–2760.
22. Issa M, Samn A. Passive vehicle suspension system optimization using Harris hawk optimization algorithm. *Math Comput Simul*. 2022;191:328-345.
23. Zhang H, Liu J, Wang E, Rakheja S, Su C. Nonlinear dynamic analysis of a skyhook-based semi-active suspension system with magneto-rheological damper. *IEEE Trans Veh Technol*. 2018;67:10446-10456.
24. Kopylov S, Chen Z, Abdelkareem M. Acceleration based ground-hook control of an electromagnetic regenerative tuned mass damper for automotive application. *Alex Eng J*. 2020;59:4933-4946.
25. Chen H, Guo K. Constrained H_∞ control of active suspensions: an LMI approach. *IEEE Trans Control Syst Technol*. 2005;13(3):412-421.
26. Yu S, Cao R, Liu Q, Qu T, Chen H. Two-layered output feedback control of energy-regenerative suspensions. *J Jilin Univ*. 2020;50:1191-1200.

27. Zeng X, Wang J. A parallel hybrid electric vehicle energy management strategy using stochastic model predictive control with road grade preview. *IEEE Trans Control Syst Technol*. 2015;23(6):2416-2423.
28. Kwon B, Kang D, Yi K. Wheelbase preview control of an active suspension with a disturbance-decoupled observer to improve vehicle ride comfort. *Proc Inst Mech Eng D J Automob Eng*. 2020;234:1725-1745.
29. Dong H, Zhao X. Wind-farm power tracking via preview-based robust reinforcement learning. *IEEE Trans Ind Inform*. 2022;18(3):1706-1715.
30. Theunissen J, Tota A, Gruber P, Dhaens M, Sorniotti A. Preview-based techniques for vehicle suspension control: a state-of-the-art review. *Annu Rev Control*. 2021;51:206-235.
31. Song S, Wang J. Incremental model predictive control of active suspensions with estimated road preview information from a lead vehicle. *J Dyn Syst Meas Control*. 2020;142(12):121004.
32. Wu J, Zhou H, Liu Z, Gu M. Ride comfort optimization via speed planning and preview semi-active suspension control for autonomous vehicles on uneven roads. *IEEE Trans Veh Technol*. 2020;69(8):8343-8355.
33. Theunissen J, Sorniotti A, Gruber P, et al. Regionless explicit model predictive control of active suspension systems with preview. *IEEE Trans Ind Electron*. 2020;67(6):4877-4888.
34. Xing X, Liu J. Event-triggered neural network control for a class of uncertain nonlinear systems with input quantization. *Neurocomputing*. 2021;440:240-250.
35. Liu Y, Liu S, Wang Y, Lombardi F, Han J. A survey of stochastic computing neural networks for machine learning applications. *IEEE Trans Neural Netw Learn Syst*. 2021;32(7):2809-2824.
36. Lin S, Zhang W. Chattering reduced sliding mode control for a class of chaotic systems. *Nonlinear Dyn*. 2018;93:2273-2282.
37. Song J, Wang Z, Niu Y, Dong H. Genetic-algorithm-assisted sliding-mode control for networked state-saturated systems over hidden Markov fading channels. *IEEE Trans Cybern*. 2021;51:3664-3675.
38. Chen F. *Study On Preview Control of Electrorheological Semi-active Suspension*. Thesis; 2017.
39. Savresi S, Poussot V, Spelta C, Sename O, Dugard L. *Semi-active Suspension Control Design for Vehicles*. Vol 17. Elsevier Technology; 2009:143-152.
40. Chen H. *Model Predictive Control*. Science Press; 2013.

How to cite this article: Yu S, Guo J, Xu M, Zhang S, Zhuang Y, Lin B. Road preview MPC of semi-active suspension with magneto-rheological damper. *Int J Robust Nonlinear Control*. 2023;1-24. doi: 10.1002/rnc.6625